Supramolecular Monolayers of Zinc Porphyrin Trimers on Graphite

J. Yin, Q. Guo,* and R. E. Palmer

Nanoscale Physics Research Laboratory, School of Physics and Astronomy, The University of Birmingham, Edgbaston, Birmingham B15 2TT, U.K.

N. Bampos and J. K. M. Sanders

Cambridge Centre for Molecular Recognition, University Chemical Laboratory, Lensfield Road, Cambridge CB2 1EW, U.K.

Received: July 10, 2002; In Final Form: November 5, 2002

Zinc porphyrin trimers have been deposited on highly oriented pyrolytic graphite (HOPG) from the liquid phase. By controlling the concentration of the solution and deposition parameters, we have prepared single molecular layers. The molecular monolayers, as characterized using both atomic force microscopy (AFM) and scanning tunneling microscopy (STM), are amorphous. The trimer molecules adopt a uniform adsorption orientation with the component porphyrin rings perpendicular to the substrate, giving rise to a monolayer film thickness of 1.7 ± 0.2 nm, which is characteristic of the height of the individual molecules. STM imaging of the molecular layers was conducted both in vacuum and in air, giving identical results. This type of molecular monolayer provides a useful platform for the study of surface and interface phenomena outside a vacuum system and is potentially useful for practical fabrication of molecular devices because of the simplicity of the sample preparation and the stability of the interface in ambient.

1. Introduction

The potential applications of molecular films in a number of important technological areas provide one of the driving forces behind fundamental studies of the molecule−substrate interactions. The prospects of producing new devices based on molecular electronics have attracted a great deal of attention from both scientists and semiconductor manufacturers.[1−4] As a result, molecular materials have already started to make an impact in industry in areas such as light-emitting diodes (LEDs), organic displays,[5−8] and thin film transistors.[1,9] Molecular materials are also potentially useful in optoelectronic applications, such as optical computing. One of the most attractive aspects of molecular materials is the possibility of synthesising designer molecules as the basic building blocks, which can then be assembled into functional structures in a way that exploits molecular recognition.

Both the structure and properties of thin molecular films depend strongly on the molecule−substrate interaction. A thorough understanding of the physics and chemistry at the molecule−substrate interface can lead to more controlled film growth for specific applications. Our understanding of molecule−substrate interactions has until very recently been largely restricted to relatively small molecules, such as benzene, but larger molecules have now entered the research scene. For instance, the adsorption of PTCDA (perylene tetracarboxylic acid dianhydride) on well-characterized single-crystal surfaces of Ag has been studied by Umbach et al. using a range of surface science techniques,[10] while the organic conductor TTF-TCNQ has also been imaged with STM.[11] Similar types of experiments have been conducted by investigators, including Bayliss et al.[12] and Upward, Beton, and Moriarty[13] with phthalocyanines, and Thomas et al.[14] and Bampos et al.[15] with porphyrins. Ordering at the molecular level has been observed for most of the molecules studied so far, and in some cases, submolecular resolution has been achieved.[16,17]

Vacuum sublimation has been the major method used for sample preparation in the surface science studies.[12,13] The advantage of this technique is that high-purity materials can be deposited in a well-controlled way, and the technique is compatible with traditional surface science techniques, which require ultrahigh vacuum. The disadvantage is that it is not practical to use this technique for molecules that decompose readily when heated. An alternative method for molecular film preparation is to use liquid-phase deposition, in which the molecules are dissolved in a solvent and then applied to a solid substrate in the form of a liquid drop. The choice of a solvent that wets the substrate completely allows a continuous ultrathin liquid film (with thickness down to the nanometer scale) to form on the surface. The spreading of the liquid film serves as a vehicle for lateral transport of the molecules on the substrate surface. Subsequent evaporation of the solvent leaves the solute molecules on the surface where they may aggregate into 2D or 3D structures, depending on molecule−substrate interactions. The morphology of the molecular film formed this way is also strongly influenced by the solvent−substrate interaction, which is absent in vacuum-based depositions. Indeed, one can take advantage of this effect to grow molecular structures not otherwise possible with vacuum sublimation. Perhaps more importantly, molecules with delicate functionalities can be deposited without fragmentation.

We report in this paper our investigations of the structure of zinc porphyrin thin films on graphite (HOPG) imaged using atomic force microscopy (AFM) and scanning tunneling microscopy (STM). A number of previous publications have reported structural analysis of various adsorbed porphyrin

* To whom correspondence should be addressed. Electronic mail: Q.Guo@bham.ac.uk. Tel.: 0121 4144657. Fax: 0121 4147327.

10.1021/jp026490u CCC: $25.00
Published on Web 12/10/2002

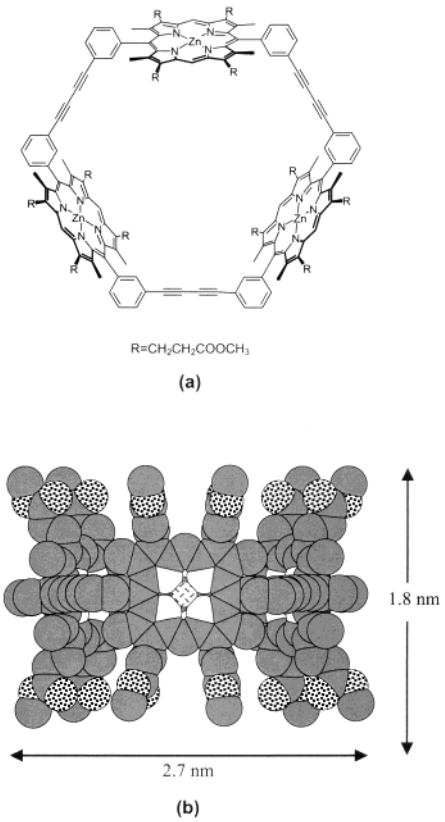

Figure 1. Molecular structure (a) of the zinc porphyrin trimer and space filling model (b) of the molecule with dimensions indicated.

molecules using STM-based techniques.[18−26] Itaya et al. have performed in situ STM studies of porphyrin adlayers on different metal electrodes[18−20] and found that ordered adlayers are formed on sulfur-modified or iodine-modified Au(111), Ag(111), and Pt(111) electrodes, while disordered adlayers of porphyrin were formed on the Au(111) surface in the absence of the iodine layer. Qiu et al.[21] demonstrated that by using substituted long-chain alkanes as molecular anchors or immobilizers both phthalocyanines and porphyrins can be immobilized at the surface of graphite to allow high-resolution STM studies. Manipulation of individual porphyrin molecules using the STM tip has been demonstrated elegantly by Gimzewski et al.,[22,23] while Moresco et al.[24,25] recently demonstrated the possibility of using a metalloporphyrin (Cu-TBPP) as a molecular switch at low temperatures. The influence of molecular functionalities on the structure of self-assembled porphyrin wires and meshes has been demonstrated recently by Yokoyama et al.[26]

In most of these previous studies, in which vacuum sublimation has been used to deposit the molecules, the adsorbed porphyrins are found to adsorb with the plane of the porphyrin ring parallel to the substrate. The measured height of the features in STM is usually in the range of ∼0.2−0.4 nm and sometimes even shows a small negative value because of electronic effects in STM imaging.[16] In our work, we used liquid-phase deposition, which allows us to deposit molecules containing delicate functional groups without fragmentation. Moreover, the zinc porphyrin trimer (ZPT) molecule used in our work has a much more complicated structure than those selected in previous studies.[18,21,22,25]

2. Experimental Section

Samples of the zinc porphyrin trimer shown in Figure 1 were prepared in Cambridge.[27] The molecule has a cavity in the middle and is composed of three butadiyne-linked diarylporphyrin monomers (Figure 1a). There are four ester side chains (which are expected to be quite flexible) substituted onto each porphyrin ring, giving a total of 12 side chains in the whole molecule. It is very difficult to obtain single crystals of this trimer suitable for X-ray diffraction analysis. However, X-ray crystallography of related diarylporphyrin monomers[28,29] indicates that the phenyl plane is nearly perpendicular to the planes of the porphyrin rings. Molecular modeling (CS ChemBats3D, CambridgeSoft, Cambridge, MA) shows that the outer diameter of the trimer cavity is 2.7 nm (Figure 1b) and the height of the trimer should be 1.8 nm.

For liquid-phase deposition of ZPT onto highly oriented pyrolytic graphite (HOPG), the molecules were first dissolved in tetrahydrofuran (THF) to make a solution with a concentration on the order of 1.0×10^{-5} M. A droplet of the solution (∼2 μL) was then applied onto a freshly cleaved HOPG surface and left to dry in air. The droplet spread evenly on the surface, resulting in the formation of a thin liquid film that covered the entire surface (10×10 mm^2). It took a few minutes for the evaporation of the solvent, leaving behind a layer of adsorbed ZPT. Any residual solvent molecules that could be trapped in the ZPT film should be removed once the sample is transferred into ultrahigh vacuum (UHV). Because the ZPT film appears the same in air and in UHV (see Results and Discussion section) as imaged using STM, the observed morphology is believed not to be influenced by residual solvent molecules if they are present at all. The concentration and volume of the solution used in the experiment were carefully chosen to ensure that the amount of porphyrin molecules deposited on the graphite surface was just about enough to form a single molecular layer. Tapping-mode AFM imaging of these thin films was performed in air at room temperature with a Dimension 3100 SPM (Digital Instruments, Santa Barbara, CA). STM imaging was performed both at room temperature in air using the Dimension 3100 and at 120 K in UHV using a variable-temperature Omicron STM. For imaging in UHV, the sample was transferred through a load lock into the UHV system with a base pressure of 4×10^{-10} mbar with no further treatment before STM imaging. Platinum/iridium tips were employed for the experiments in air, while an electrochemically etched tungsten tip was used for imaging in UHV.

3. Results and Discussion

3.1. Morphology of the ZPT Films and the Molecular Orientation. The concentration of porphyrin trimers in the solution has a strong effect on the morphology of the molecular films formed on graphite. Figure 2 shows four AFM images of porphyrin films prepared using solutions with concentrations from 4.6×10^{-6} to 1.2×10^{-4} M. In the case of the solution of the lowest concentration, the porphyrin film covers about 50% of the graphite substrate, as shown in Figure 2a. The darker areas in the image are bare graphite substrate, while the lighter areas correspond to the ZPT film. The height difference between the darker and the lighter areas, as measured with AFM, is 1.5 nm, which is a measure of the film thickness. The true film thickness is expected to be slightly different from this value because the height difference measured by AFM is dependent on the force applied. Moreover, the surface of the molecular film is not atomically smooth and shows a height variation of about 2 Å. As the concentration of the solution increases (Figure 2b,c), the fraction of the bare graphite substrate is reduced and eventually the substrate is covered by nearly a complete layer of ZPT, Figure 2c. The measured film thickness remains

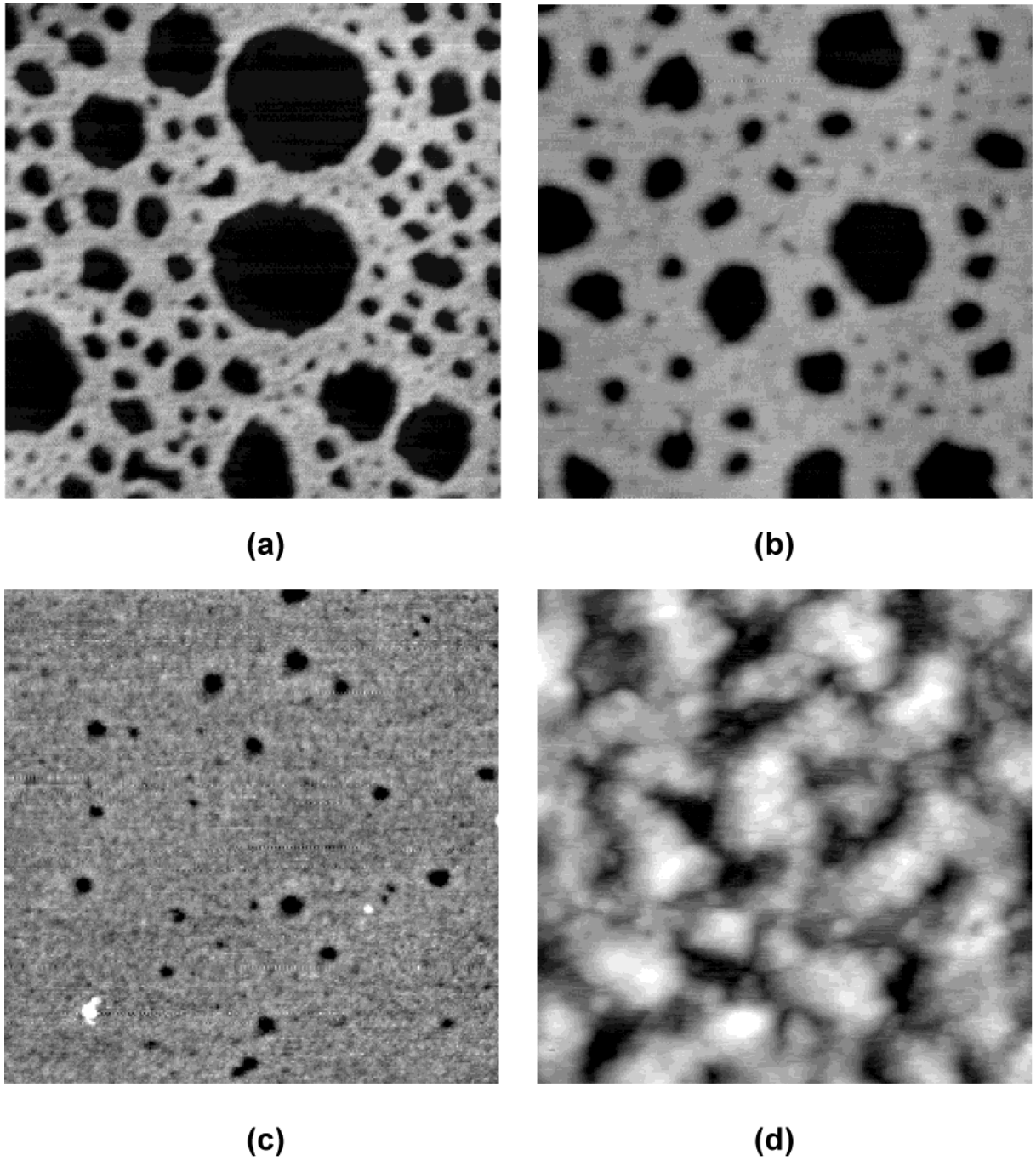

Figure 2. Tapping mode AFM images (1 × 1 μm^2 in all cases) of ZPT monolayer films prepared on graphite with different solution concentrations: (a) 4.6×10^{-6}; (b) 1.2×10^{-5}; (c) 2.9×10^{-5}; (d) 1.2×10^{-4} M.

unchanged as the molecular coverage increases from the submonolayer regime toward one full monolayer. With even higher solution concentrations, the morphology of the film changes dramatically, Figure 2d. The flat film is now replaced by irregular structures that are 5−6 nm above the substrate surface, corresponding to multilayer islands. In the rest of the paper, we will concentrate on the properties of the smooth but incomplete monolayer-high films prepared using a solution concentration of 1.2×10^{-5} M, as shown in Figure 2b. With this concentration, the image shown in Figure 2b is representative of nearly the whole sample surface apart from small fractions of the surface near the edge of the sample. Very slight variations in the average hole size have been noticed when images are acquired from different regions of the sample. A possible reason for this is local variation in film thickness due to, for example, nonuniform evaporation rates.

The morphology of the ZPT film shown in Figure 2a closely resembles that observed as a result of dewetting processes in thin liquid films.[30a] It is known that in thin liquid films holes are formed because of rupture of the film induced either by defects (at the surface or in the film[31]) or by spontaneous rupture caused by capillary waves. The latter is known as spinodal dewetting.[32] The larger holes in Figure 2a are probably formed at an early stage of the drying process when the liquid film is thick and then expand with time. The smaller holes are probably formed when the liquid film is very thin and do not have time to expand laterally because of rapid evaporation of the solvent. This seems to be consistent with the broad hole-size distribution

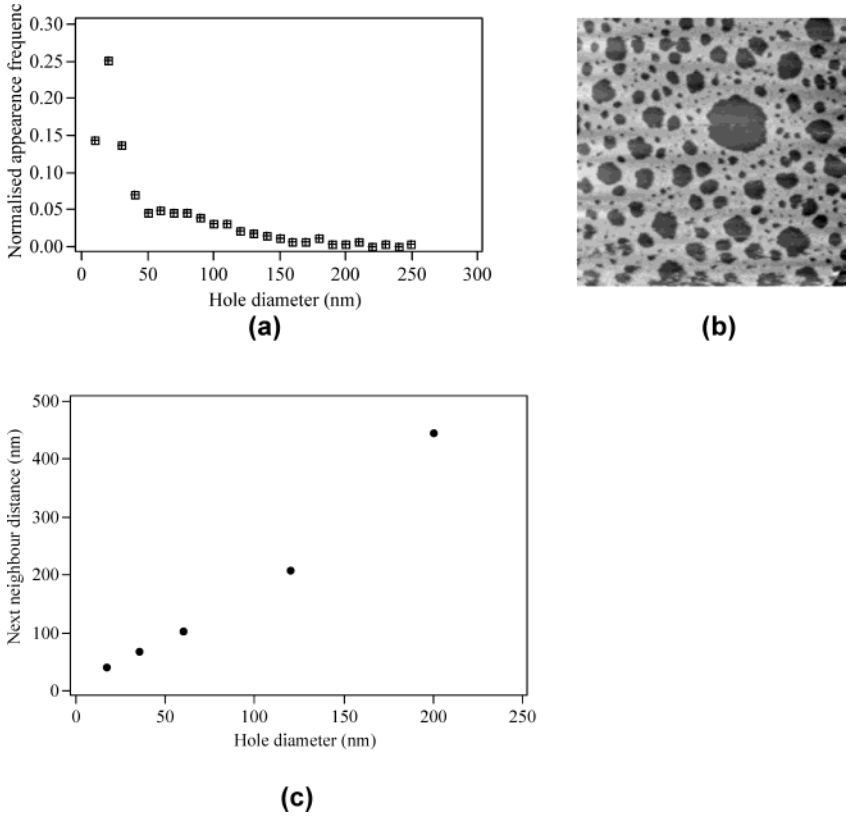

Figure 3. Normalized appearance frequency (a) of holes based on the STM image ($2.5 \times 2.5\ \mu m^2$) shown in panel b. Panel c shows the average next neighbor distance plotted against the hole diameter. Only distances between two neighboring holes of the same diameter range are measured.

observed in the experiments. Most published works on dewetting at the liquid−solid interface are focused on liquid films of a time-invariant thickness in which spinodal dewetting can be identified from the formation of a regular pattern of undulations with a characteristic "wavelength". In our case, the thinning of the liquid film competes with the formation and a expansion of the dry spots. As a result, holes formed at different times have different time interval to grow before the complete evaporation of the solvent. Therefore, it is not as straightforward to establish whether spinodal dewetting occurs. Figure 3a shows the appearance frequency of holes, normalized to the total number of holes within a $2.5 \times 2.5\ m^2$ area. This plot is based on the STM image (details of STM imaging in next section) shown in Figure 3b. An STM image, rather than an AFM image, is used for appearance frequency analysis because it offers a higher lateral resolution. To obtain the plot in Figure 3a, the diameters of all of the holes in this STM image are measured and grouped in 10 nm steps. The number of each group is then normalized to the total number of holes and plotted against the diameter of the holes. There is a narrow peak at around 20 nm and a very long tail toward larger diameters. A bump can be seen at around 70−80 nm, but because of limited statistics (286 holes in total counted), the curve shown in Figure 3a cannot be convincingly claimed to be a bimodal distribution. What is certain is that apart from the narrow peak at 20 nm, the size distribution of holes is very broad. The average distance between neighboring holes of the same diameter group has also been obtained, and the result shown in Figure 3c. It is clear that the distance increases with the diameter of the holes, that is, smaller holes are separated by shorter distances. This seems to be consistent with a spinodal dewetting mechanism, which predicts that for holes formed at the same time the hole−hole separation is proportional to the square of the film thickness. It is important to point out that dewetting under continuous film thinning is a rather complicated dynamical process. In our case, as holes are formed and expand, the surface tension, as well as the viscosity, of the remaining liquid film changes accordingly because of an increased ZPT concentration. This, in turn, will affect the subsequent formation and growth of dry spots.

It is clear that surface defects on graphite do not play a role in the formation of the dry spots. The most prominent defects on graphite surfaces are step edges; however, we do not observe any specific alignment of the holes along step edges. Thermal fluctuations in the solvent may cause localized surface stress within the liquid film, leading to film rupture at random locations such as that reported recently in polymer films.[30b] The structure of the thin ZPT films shown in Figure 2a−c indicates that the ZPT−graphite interaction is rather weak. For instance, no isolated ZPT molecule is found inside the vacancy islands, that is, the solvent−ZPT interaction is strong enough that the molecules are carried to wherever the liquid moves. Therefore, the resulting morphology of the deposited ZPT film is determined mostly by the shape of the liquid film at the last stage of drying.

The temperature dependence of the morphology of the ZPT film has been investigated by annealing the ZPT film up to 570 K in vacuum and in nitrogen. Figure 4 shows three AFM images of a ZPT film before and after annealing to 470 and 570 K in a vacuum. The images were not from exactly the same area of the sample because the sample was moved from the AFM to the annealing apparatus between image acquisitions. While the images in Figure 4a,b appear quite similar, annealing has clearly caused changes to the ZPT monolayer. The shape of the holes has changed upon annealing, and the boundary of the holes becomes jagged suggesting that edge diffusion occurred. Moreover, complete or partial hole coalescence is also evident from the image. Annealing to 570 K causes partial desorption of the ZPT film, as shown in Figure 4c. The image in Figure

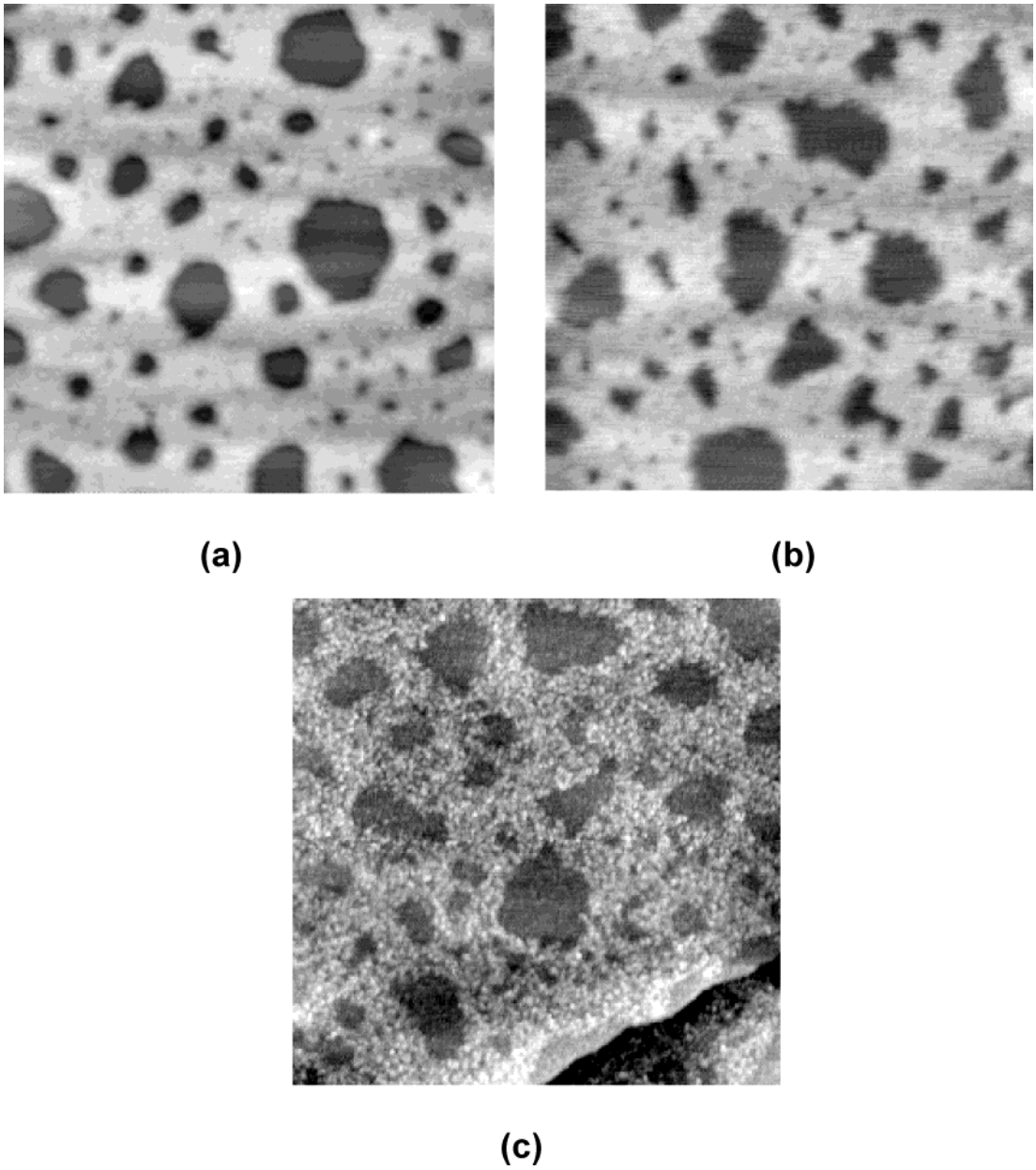

Figure 4. AFM images ($1 \times 1\ \mu m^2$) of a ZPT film before (a) and after annealing in vacuum to (b) 470 and (c) 570 K.

4c shows a decreased molecular density and a reduction of the film thickness to 0.6 nm, which is comparable to the film thickness of the corresponding zinc porphyrin monomers.[33] Thus, the cyclic trimers may have been fragmented into the monomer constituents upon heating to 570 K, although a structural change from a more dense to a loosely packed film can also lead to a lowering of the height in AFM measurements.

The ZPT film was also imaged using STM, both in ambient atmosphere at room temperature and in UHV at cryogenic temperatures. Figure 5a shows a typical image obtained at 120 K in UHV. A similar STM image obtained in air at room temperature is shown in Figure 5b for comparison. It can be seen that both STM images are very similar to the AFM images shown in Figure 2. The possibility to image the molecular film in air using the STM is rather valuable because most molecular films prepared in vacuum cannot be imaged in air due to degradation of the molecules or the oxidation of the substrates. The fine scale texture of the ZPT monolayer is revealed in the STM image shown in Figure 5c. This image was obtained at 120 K in vacuum, and the scattered loose molecules seen inside two of the dark circular areas are due to displaced molecules caused by previous scans in the central part of the image. The grainy appearance of the molecular monolayer is directly associated with the ZPT molecules.

Despite the lack of long-range order within the molecular monolayer, the individual ZPT molecules appear to have a preferred orientation on the surface as shown in the STM image of Figure 5d. It can be seen in this image that the molecular film is porous. By careful examination of the image, one can see ring-like features within the monolayer. One of these features is shown as inset (A) in Figure 5d. These rings are not exactly circular, and their "diameter" is around 2.5 nm, which is close to the lateral dimension of the ZPT molecule (Figure 1b). The lack of order within the monolayer makes it difficult to correlate the lateral positions of the molecules; however, the identification of the ring-like features leads to the determination of the orientation of these molecules relative to the substrate surface. Although the ZPT molecule could take several orientations on the surface, the only one that is consistent with the STM observation is the one with the molecules standing on either

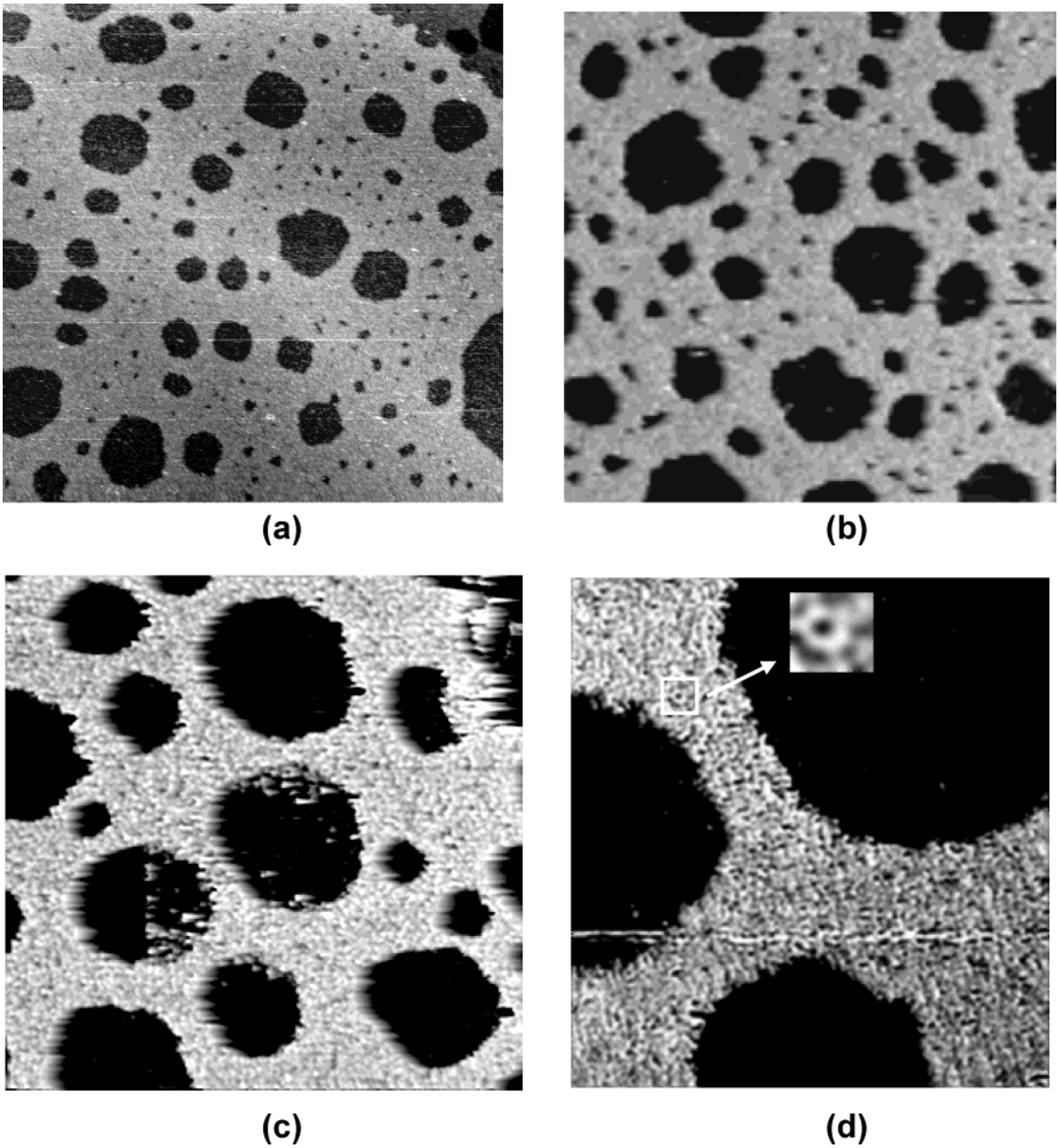

Figure 5. STM images of ZPT monolayer films on graphite: (a) STM image ($1 \times 1\ \mu m^2$) obtained in UHV at 120 K with tunneling parameters $V = 3.5$ V and $I = 27$ pA; (b) STM image ($1 \times 1\ \mu m^2$) obtained at room temperature in air with tunneling parameters $V = 1.74$ V and $I = 27$ pA; (c) STM image (500×500 nm^2) obtained in UHV at 120 K with tunneling parameters $V = 2.5$ V and $I = 40$ pA; (d) fine scale STM image (200×200 nm^2) obtained in UHV with same parameters as those in panel c. Inset A shows the image arising from an individual ZPT molecule.

the upper or the lower group of the six ester chains as depicted in Figure 1b. The plane of the three porphyrin rings within each ZPT molecule is thus perpendicular to the substrate. The height of the molecular layer, measured with the STM, is 1.85 nm, which is in good agreement with the height of the molecule in this orientation (see Figure 1b). With this kind of adsorption geometry, it is ideally expected that each ZPT molecule shows three spots in STM images due to the symmetry of the molecule. Such a three-spots-like structure can be seen in Figure 5d. However, because of the weak intermolecular and molecular−substrate interactions, the molecules possess a high degree of freedom, as will be shown in the following section. Because of this degree of freedom, the molecules can translate and rotate on the surface, making high-resolution STM imaging very complicated.

A direct consequence of the high degree of freedom of the molecules is that the molecules can be easily moved around by the STM tip under normal imaging conditions. For instance, scanning the same area repeatedly four or five times under normal tunneling conditions (2.0−3.0 V and 30 pA) at room temperature results in a complete change of the surface morphology. Figure 6a shows an STM image taken in air illustrating the effect of the tip on the surface morphology of the ZPT film. The area marked with a square ($2 \times 2\ \mu m^2$) had been scanned five times, after which a clear change in the image became apparent in the larger area image ($5 \times 5\ \mu m^2$) shown in Figure 6a obtained with the same tunneling parameters. It is evident from Figure 6a that the characteristic structure of the ZPT films has been completely destroyed inside the square by the STM tip. No piling up of molecules was observed at the boundaries of the marked square, so we cannot conclude that the molecules are pushed aside by the tip; some ZPT molecules may instead have transferred to the tip as has been observed in scanning a film of passivated Au clusters.[34]

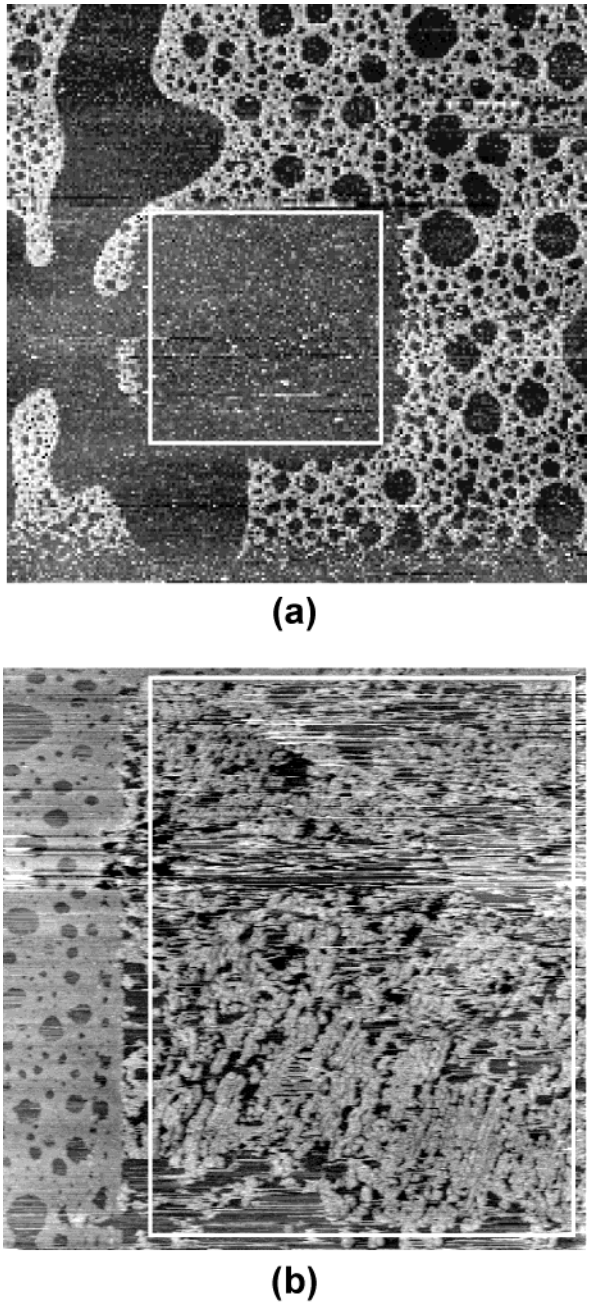

Figure 6. STM images showing tip-induced modifications of the ZPT film. Panel a shows an image ($5 \times 5\ \mu m^2$) obtained at room temperature in air ($V = 2.4$ V, $I = 50$ pA). The area within the marked square has previously been scanned five times at 2.4 V and 50 pA. Panel b shows an image ($2 \times 2\ \mu m^2$) obtained at 330 K in UHV ($V = 3.1$ V, $I = 72$ pA). The area inside the rectangle has previously been scanned once with 3.1 V and 72 pA.

The modification of the ZPT film with the STM appears to be a combined effect of the tip and temperature. At 120 K in UHV, the film was not affected at all by repeated scanning. By increasing the temperature of the sample in UHV slowly, we found that modification of the ZPT film began at 309 K, while above 330 K, no stable image could be obtained because of rapid changes within the film. Figure 6b illustrates the tip-induced changes to the ZPT film at 330 K in UHV. The area within the white rectangle has been modified with a single scan using normal scanning parameters ($V = 3.1$ V, $I = 72$ pA). The tip was then offset to the left by 450 nm, and the image shown in Figure 6b was taken with the same parameters. During image acquisition, a clear boundary line was observed in the image dividing the fresh area and the area that has been scanned once previously. To the left of the boundary line, the surface shows typical morphology of adsorbed ZPT layer, while to the right of the line, the initial structure of the ZPT layer is totally transformed by the previous scan. It was noted that the structure to the left side of the boundary line changed to a similar structure to that on the right when the same area was scanned again. Therefore, a single scan with the parameters used is sufficient to cause significant modifications of the ZPT film. In contrast to the image shown in Figure 6a (modification in the ambient at room temperature), the modified area is still covered by ZPT molecules, although they are now more loosely packed. It is thus apparent that tip-induced film modification in UHV leads to different surface structures than modifications in the ambient. The molecules appear to be dragged laterally by the tip from their initial positions to fill the vacant holes. In the air, most of the molecules within the modified area seem to have transferred to the tip. Water vapor at the tunneling junction may facilitate the transport of molecules onto the tip in air.

In view of the adsorption orientation proposed here, the bonding between the ZPT molecule and the graphite surface is dominated by the interaction of the six ester chains with the surface carbon atoms. Each CH_3 group at the end of an ester chain would provide ~70 meV of adsorption energy,[35] so the total adsorption energy of a ZPT molecule would be at least 0.42 eV. Apart from the CH_3 groups, the rest of the molecule can interact "through space" via van der Waals forces. In addition, the molecular film can also be stabilized through intermolecular interactions.

3.2. Tunneling Mechanism. The electron tunneling mechanism in STM imaging of biological and organic molecules is complicated; indeed, in many cases, the conductivity seems to be too low to allow good imaging, resulting in measured heights that are much smaller than the geometric size of the molecule.[36] For instance, self-assembled monolayers of dodecanethiol adsorbed on gold have a layer thickness of 1.2 nm. However, STM measurements give a monolayer height of only 1.8 Å above the substrate.[37,38] In the case of copper−tetra-3,5-di-*tert*-butyl phenyl porphyrin (Cu−TBPP) adsorbed on the Cu(211) surface, the measured height of the molecule is 2 Å, which is much less than the expected value of 11 Å.[26] The much lower value of the measured height of the molecules is either due to a much higher tunnel barrier above the molecules or due to a poor conductivity associated with the molecules. The height of the ZPT molecules adsorbed on graphite as measured with the STM in this work is in very good agreement with the geometric height of the molecule. This suggests that the tunnel barrier above the molecules is comparable to that of the graphite substrate and that the conductivity of the molecules is high enough not to limit the tunneling current. However, this is valid provided the gap voltage is high enough (>1.5 V). At lower bias voltages, the ZPT molnolayer behaves as an insulating film.[39] Because the LUMO−HOMO gap of ZPT molecules is 2.2 eV, it is envisaged that tunneling may involve the injection of electrons into the LUMO of the molecules. At present, there is a lack of detailed understanding of electron transport through this type of molecules, and therefore, a full understanding of the tunneling mechnism has to wait until further investigations.

4. Conclusions

In conclusion, we have prepared monolayers of zinc porphyrin trimers on graphite by liquid-phase deposition and imaged the molecular films with both AFM and STM. The molecular film is in the form of a nanoporous amorphous state. Individual ZPT

molecules adopt a uniform orientation relative to the graphite surface with the porphyrin rings perpendicular to the substrate. The height of the molecular monolayer measured by STM is in good agreement with the height of the ZPT molecule, suggesting that the tunneling barrier presented by the molecules is comparable to that of graphite under the bias voltage applied. The molecular film is stable enough to allow STM imaging in air, presenting itself as a useful platform for surface science research outside of a vacuum system.

Acknowledgment. This work is supported by the LeverhulmeTrust and the UK EPSRC.

References and Notes

(1) Carter, F. L., Siatowski, R. E., Wholtjen, H., Eds. *Molecular Electronic Devices*; North-Holland: Amsterdam, 1988.
(2) Aviram, A., Ed. *Molecular Electronics*: *Science and Technology*; Engineering Foundation: New York, 1989.
(3) Drury, C. *Appl. Phys. Lett*. **1998**, *73*, 108.
(4) Garnier, F.; Hajlaoui, R.; Yassar, A.; Srivastava, P. *Science* **1994**, *265*, 1684.
(5) Kido, J.; Kimura, M.; Nagai, K. *Science* **1995**, *267*, 1332.
(6) Burroughes, J. H.; Bradley, D. D. C.; Brown, A. R.; Marks, R. N.; Mackay, K.; Friend, R. H.; Burn, P. L.; Kraft, A.; Holmes, A. B. *Nature* **1990**, *347*, 530.
(7) Greenham, N. C.; Moratti, S. C.; Bradley, D. D. C.; Friend, R. H.; Holmes, A. B. *Nature* **1993**, *365*, 628.
(8) Braun, D.; Heeger, A. J. *Appl. Phys. Lett*. **1991**, *58*, 1982.
(9) Bao, Z.; Dodabalapur, Z. A.; Lovinger, A. J. *Appl. Phys. Lett*. **1996**, *69*, 4108−4110.
(10) Umback, E.; Glckler, K.; Sokolowski, M. *Surf. Sci*. **1998**, *402*−*404*, 20.
(11) Sleator, T.; Tycko, R. *Phys. Rev. Lett*. **1988**, *60*, 1418.
(12) Bayliss, S. M.; Heutz, S.; Rumbles, G.; Jones, T. S. *Phys. Chem. Chem. Phys*. **1999**, *1*, 3673.
(13) Upward, M. D.; Beton, P. H.; Moriarty, P. *Surf. Sci*. **1999**, *441*, 21.
(14) Thomas, P. J.; Berovic, N.; Laitenberger, P.; Palmer, R. E.; Bampos, N.; Sanders, J. K. M. *Chem. Phys. Lett*. **1998**, *294*, 229.
(15) Bampos, N.; Woodburn, C. N.; Welland, M. E.; Sanders, J. K. M. *Angew. Chem., Int. Ed*. **1999**, *38*, 2780.
(16) Gimzewski, J. K.; Jung, T. A.; Cuberes, M. T.; Schlittler, R. R. *Surf. Sci*. **1997**, *386*, 101.
(17) Furukawa, M.; Tanaka, H.; Sugiura, K.; Sakata, Y.; Kawai, T. *Surf. Sci*. **2000**, *445*, L58.
(18) Wan, L.-J.; Shundo, S.; Inukai, J.; Itaya, K. *Langmuir* **2000**, *16*, 2164.
(19) Sashikata, K.; Sugata, T.; Sugimasa, M.; Itaya, K. *Langmuir* **1998**, *14*, 2896.
(20) Kunitake, M.; Akiba, U.; Batina, N.; Itaya, K. *Langmuir* **1997**, *13*, 1607.
(21) Qiu, X.; Wang, C.; Zeng, Q.; Xu, B.; Yin, S.; Wang, H.; Xu, S.; Bai, C. *J. Am. Chem. Soc*. **2000**, *122*, 5550.
(22) Gimzewski, J. K.; Joachim, C. *Science* **1999**, *283*, 1683.
(23) Jung, T. A.; Schlittler, R. R.; Gimzewski, J. K.; Tang, H.; Joachim, C. *Science* **1996**, *271*, 181.
(24) Moresco, F.; Meyer, G.; Rieder, K.-H.; Tang, H.; Gourdon, A.; Joachim, C. *Appl. Phys. Lett*. **2001**, *78*, 306.
(25) Moresco, F.; Meyer, G.; Rieder, K.-H.; Tang, H.; Gourdon, A.; Joachim, C. *Phys. Rev. Lett*. **2001**, *86*, 672.
(26) Yokoyama, T.; Yokoyama, S.; Kamikado, T.; Okuno, Y.; Mashiko, S. *Nature* **2001**, *413*, 619.
(27) Bampos, N.; Marvaud, V.; Sanders, J. K. M. *Chem.—Eur. J*. **1998**, *4*, 335.
(28) Bampos, N.; Prinsep, M. R.; He, H.; Vidal-Ferran, A.; Bashall, A.; McPartlin, M.; Powell, H.; Sanders, J. K. M. *J. Chem. Soc*., *Perkin Trans*. **1998**, *2*, 715.
(29) Bond, A. D.; Feeder, N.; Redman, J. E.; Teat, S. T.; Sanders, J. K. M. *Cryst. Growth Des.* **2002**, *2*, 29.
(30) (a) Thiel, U.; Mertig, M.; Pompe, W. *Phys. Rev. Lett*. **1998**, *80*, 2869. (b) Masson, J.-L.; Green, P. F. *Phys. Rev. Lett*. **2002**, *88*, 205504-1.
(31) Kheshgi, H. S.; Scriven, L. E. *Chem. Eng. Sci*. **1991**, *46*, 519.
(32) Brochard, F.; Daillant, J. *Can. J. Phys*. **1990**, *68*, 1084.
(33) Yin, J.; Guo, Q.; Palmer, R. E.; Bampos, N.; Sanders, J. K. M. *Surf. Sci*., submitted for publication.
(34) Durston, P. J.; Palmer, R. E.; Wilcoxon, J. P. *Appl. Phys. Lett*. **1998**, *72*, 176.
(35) Hentschke, R.; Schurmann, B. L.; Rabe, J. P. *J. Chem. Phys*. **1992**, *96*, 6213.
(36) Guckenberger, R.; Heim, M.; Cevc, G.; Knapp, H. F.; Wiegrabe, W.; Hillebrand, A. *Science* **1994**, *266*, 1538.
(37) Poirier, G. E.; Pylant, E. D. *Science* **1996**, *72*, 1145.
(38) Guo, Q.; Sun, S.; Chen, Y.; Palmer, R. E. *Surf. Sci*. **2002**, *497*, 269.
(39) Palmer, R. E.; Guo, Q. *Phys. Chem. Chem. Phys*. **2002**, *4*, 4275.